Inorganica Chimica Acta 390 (2012) 83–94

Contents lists available at SciVerse ScienceDirect

Inorganica Chimica Acta

journal homepage: www.elsevier.com/locate/ica

Reactions of N-heterocyclic ligands with substitutionally labile organometallic complexes, $[(\eta^5\text{-}C_5R_5)Fe(CO)_2E]BF_4$

Cyprian M. M'thiruaine [a], Holger B. Friedrich [a,*], Evans O. Changamu [b], Muhammad D. Bala [a]

[a] School of Chemistry, University of KwaZulu-Natal, Private Bag X54001, Durban 4000, South Africa
[b] Chemistry Department, Kenyatta University, P.O. Box 43844, Nairobi, Kenya

ARTICLE INFO

Article history:
Received 21 October 2011
Received in revised form 29 March 2012
Accepted 1 April 2012
Available online 7 April 2012

Keywords:
N-heterocyclic iron complexes
1-Methylimidazole
1,3,5,7-Tetraazaadamantane
1,4-Diazabicyclo[2.2.2]octane

ABSTRACT

The ether complexes $[Cp(CO)_2Fe(OEt_2)]BF_4$ (Cp = η^5-C_5H_5) (**1**) and $[Cp^*(CO)_2Fe(THF)]BF_4$ (Cp^* = η^5-$C_5(CH_3)_5$) (**2**) react with 1,3,5,7-tetraazaadamantane (HMTA) to give stable water-soluble dinuclear complexes $[\{(\eta^5\text{-}C_5R_5)(CO)_2Fe\}_2(\mu\text{-HMTA})](BF_4)_2$ (R = H; R = CH_3) and mononuclear complexes $[(\eta^5\text{-}C_5R_5)(CO)_2Fe(HMTA)]BF_4$ (R = H; R = CH_3). The reaction of **1** with 1,4-diazabicyclo[2.2.2]octane (DABCO) gave good yields of the dinuclear and mononuclear complexes, $[\{Cp(CO)_2Fe\}_2(\mu\text{-DABCO})](BF_4)_2$ (**6a**) and $[Cp(CO)_2Fe(DABCO)]BF_4$ (**6b**), respectively, depending on reagent ratios. Similar reactions with **2** gave very low yields of the mononuclear complex $[Cp^*(CO)_2Fe(DABCO)]BF_4$ (**6c**) as the only product. The reactions of $[Cp(CO)_2Fe(HMTA)]BF_4$ (**3b**) and $[Cp^*(CO)_2Fe(HMTA)]BF_4$ (**4b**) with $NaBPh_4$ in acetone proceeded smoothly at room temperature to give the corresponding BPh_4^- salts. Reaction of **4b** with **1** at room temperature gave the dinuclear complex $[\{Cp(CO)_2Fe\}_2(\mu\text{-HMTA})](BF_4)_2$ (**3a**) as the major product, while the same reaction conducted at 0 °C led to the unstable mixed ligand complex $[\{Cp(CO)_2Fe\}(\mu\text{-HMTA})\{Fe(CO)_2Cp^*\}](BF_4)_2$. The reactions of **1** and **2** with 1-methylimidazole (1-meIm) gave high yields of $[(\eta^5\text{-}C_5R_5)(CO)_2Fe(1\text{-meIm})]BF_4$ (R = H (**7**); R = CH_3 (**8**)), of which the NMR, IR and single crystal X-ray studies reveal the coordination of 1-methylimidazole to be via the 'pyridine nitrogen' of the imidazole ring. Single-crystal X-ray diffraction studies reveal that compounds **3a** and **8** crystallize in the orthorhombic $P2_12_12_1$ and $Pna2_1$ space groups, respectively. Compound **7** however, crystallized in the monoclinic $P2_1/c$ space group with three independent molecular cations and anions each in the asymmetric unit.

1. Introduction

In recent years, there has been a great deal of interest in complexes bearing cage-like 1,3,5-triaza-7-phosphaadamantane (PTA) [1–6] due to its ability to solubilize metal complexes in the aqueous phase [7,8]. Some of these complexes have found application in aqueous phase and biphasic catalytic systems [9–13] as well as in pharmaceuticals [5,7]. The synthesis of water-soluble organometallic derivatives has been widely achieved by the design of water-soluble ligands that, when incorporated into the coordination sphere of the metal, impart water-solubility to the complexes. The solubilizing ability of the PTA complexes for instance is imparted by the nitrogen atoms which form hydrogen bonds with water molecules.

PTA and other N-based aromatic heterocycles have also been widely used as metal coordination spacers owing to their good donor ability and rigidity [14–16]. HMTA and its derivatives, in particular, have been used as antibacterial agents in the treatment of urinary tract infections since 1932 [17–19], and their anti-bacterial activity has been the subject of many patents in recent years. For example, methenamine (HMTA), methenamine anhydromethylene-citrate, methenamine hippurate, methenamine mandelate and methenamine sulfosalicylate have all been reported as synthetic antibacterials [20] and as anti-infectives [21]. HMTA has also been applied in the treatment of ear canal infections in combination with anti-inflammatory and antiseptic agents [22], and as an adjuvant to radiation and cisplatin in the treatment of solid tumors [23]. In recent years HMTA has been used as base catalyst in the synthesis of phenolic gel and most recently García et al. published a report on the use of HMTA as a base catalyst to control the porosity and pore size of resorcinol furaldehyde cryogels synthesized in *t*-butanol [24].

DABCO is known mainly as an organic catalyst in a large variety of organic syntheses [25–27]. For example it has displayed high catalytic activity in the methylation of indole in conjunction with dimethyl carbonate [28]. Gordon et al. have demonstrated that DABCO derivatives can also be used as Voltage-Gated potassium channel blockers [29]. To the best of our knowledge, the DABCO iron complexes of the type $[(CO)_4Fe(DABCO)]$ and $[\{(CO)_4Fe\}_2(\mu\text{-DABCO})]$ are the only reported iron carbonyl complexes incorporating the DABCO ligand in the coordination sphere [30].

* Corresponding author. Tel.: +27 312603107; fax: +27 312603109.
E-mail address: friedric@ukzn.ac.za (H.B. Friedrich).

0020-1693/$ - see front matter © 2012 Elsevier B.V. All rights reserved.
http://dx.doi.org/10.1016/j.ica.2012.04.003

1-Methylimidazole (1-meIm) is a derivative of imidazole (Im) which also finds application in drug design [31,32] and catalysis [32,33]. This has instigated interest in coordination of imidazole-based ligands to transition metals [34] leading to the reporting of a wide variety of imidazole transition metal complexes [35,36]. This includes the complexes $[Cp(CO)_2FeL\text{-}BPh_3]$ (L = imidazole, benzimidazole) reported by Nesmayanov et al. as a product of the decomposition reaction of the salts $[Cp(CO)_2FeLH]^+$ BPh_4^- [35]. A ligand substitution reaction could be an alternative route to the cationic complex $[Cp(CO)_2FeL]^+$, whereby labile ligands such as THF, Et_2O or acetone are replaced by the imidazole ligand. However, such reactions have not been previously reported.

The importance of N-heterocyclic ligands in physiology, pharmaceuticals and catalysis, as well as interest in exploration of the coordination chemistry of amine ligands, aroused our interest in the coordination of such ligands to transition metal centres of varying electronic and steric environments. This may enhance an understanding of their interactions with a metal ion and, hence, provide models for active anti-bacterials or catalysts. For this report, iron was the metal of choice since it is relatively non-toxic, inexpensive and easy to handle due to the high stability exhibited by its complexes. Moreover, iron complexes with bidentate *N*,*N*-ligands and tridentate *N*,*N*,*N*-ligands have been shown to catalyse ethylene oligomerization and polymerization reactions [37–40]. Iron is also found in the blood of both vertebrates and invertebrates in which it forms Fe–N bonds in the *heme* group of hemoglobin or myoglobin. To the best of our knowledge HMTA, DABCO and 1-meIm complexes with the $\{(\eta^5\text{-}C_5R_5)(CO)_2Fe\}$ moiety are unknown. Herein, we report the syntheses and characterization of the novel complexes of the types, $[\{(\eta^5\text{-}C_5R_5)(CO)_2Fe\}_2L)](BF_4)_2$ and $[(\eta^5\text{-}C_5R_5)(CO)_2FeL]BF_4$ (R = H, CH_3; L = HMTA, DABCO) as well as $[(\eta^5\text{-}C_5R_5)(CO)_2Fe(1\text{-meIm})]BF_4$ (R = H, CH_3; 1-meIm = 1-methylimidazole), which is a part of an on-going study on functionalized transition metal alkyl complexes [41–48].

2. Results and discussion

The three N-heterocyclic ligands employed in this investigation react with the ether complexes $[Cp(CO)_2Fe(OEt_2)]BF_4$ (**1**) and $[Cp^*(CO)_2Fe(THF)]BF_4$ (**2**) at room temperature in dichloromethane to afford complexes **3**–**8** as shown in Scheme 1. The N-heterocyclic ligands are generally good electron donors and therefore readily displace weakly bound Et_2O and THF molecules. All the complexes were obtained in moderate to excellent yields as yellow to orange solids, except for compound **6c** which was obtained in a low yield. They are fairly stable in air but slowly decompose when in solution and particularly when exposed to light. For this reason, manipulations of the compounds in solution were done in the dark under strictly anaerobic conditions. The complexes have been fully characterized by elemental analysis, NMR and IR spectroscopy (Sections 4.2–4.12) as well as single crystal X-ray diffraction. Mass spectroscopy data of compounds **3a**, **4b**, **6b** and **8** have also been recorded in 100% water.

2.1. Reaction of hexamethylenetetramine (HMTA) with the ether complexes $[(\eta^5\text{-}C_5R_5)(CO)_2Fe(E)]BF_4$ (R = H, E = Et_2O (**1**), R = CH_3, E = THF (**2**))

1,3,5,7-Tetraazaadamantane (commonly known as hexamethylenetetramine and abbreviated HMTA), readily reacts with **1** at room temperature to give the dinuclear complex **3a** and the mononuclear complex **3b**. Similarly, the reaction of HMTA with **2** yields the dinuclear complex **4a** and the mononuclear complex **4b** whether the dinuclear or the mononuclear complex is isolated depends on the stoichiometric ratio of the reagents employed. Thus, the reaction of the etherate complexes with a slight excess of HMTA furnished only the mononuclear product, while 1:1 or 2:1 mol ratios (etherate complex to HMTA) gave mixtures of dinuclear $[\{(\eta^5\text{-}C_5R_5)(CO)_2Fe\}_2(\mu\text{-HMTA})](BF_4)_2$ and mononuclear $[(\eta^5\text{-}C_5R_5)(CO)_2Fe(HMTA)]BF_4$ (R = H, CH_3) complexes as products with the relative amount of the mononuclear product decreasing with increase in etherate reactant used in the reaction. When the mole ratio of the reaction is raised to 4:1, only the dinuclear complex $[\{(\eta^5\text{-}C_5R_5)(CO)_2Fe\}_2(\mu\text{-HMTA})](BF_4)_2$ was isolated. No evidence for the formation of the tetranuclear complex $[\{(\eta^5\text{-}C_5R_5)(CO)_2Fe\}_4(\mu_4\text{-HMTA})](BF_4)_4$ was obtained, even when large excesses of the etherate complexes were employed. This is probably due to the steric hindrance induced by the two $\{(\eta^5\text{-}C_5R_5)(CO)_2Fe\}$ groups occupying two of four binding sites of the HMTA ligand.

The mononuclear complexes were obtained as yellow, while the dinuclear complexes were obtained as orange solids. All the complexes were soluble in water, acetone and acetonitrile. The complexes **4a** and **4b** were also soluble in dichloromethane and were easily isolated from solution by precipitation using diethyl ether. It was difficult to separate the dinuclear from the mononuclear compounds, thus pure samples of the dinuclear and mononuclear compounds were obtained by using the appropriate mole ratios of the reactants.

The IR spectra of compounds **3a**–**4b** show two strong absorption bands in the range 2058–1982 cm^{-1} assignable to the two terminal carbonyls as expected for cationic amine complexes [44,48–50]. The IR spectra of **4a** and **4b** exhibited characteristic ν(CO) stretching vibrations at wavenumbers lower than those of **3a** and **3b** by *ca.* 21 cm^{-1}, which is due to the enhanced back-donation of metal to carbon as a result of the electron rich $C_5(CH_3)_5$ ligand. A characteristic band due to CN stretching of HMTA was observed at 1227–1244 cm^{-1} as expected [51]. The ν(CO) vibrations of the mononuclear complexes were not significantly different from those of the dinuclear complexes and therefore it was not possible to distinguish the mononuclear from the dinuclear

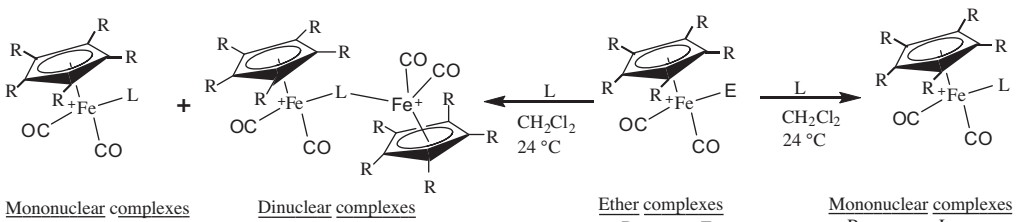

Mononuclear complexes

	R	L
3b	H	HMTA
4b	CH_3	HMTA
6b	H	DABCO
6c	CH_3	DABCO

Dinuclear complexes

	R	L
3a	H	HMTA
4a	CH_3	HMTA
6a	H	DABCO

Ether complexes

	R	E
1	H	Et_2O
2	CH_3	THF

Mononuclear complexes

	R	L
7	H	1-meIm
8	CH_3	1-meIm

Scheme 1. Reactions of etherate complexes **1** and **2** with N-heterocyclic ligands.

complexes based solely on carbonyl vibration frequency. However, the IR spectra of the mononuclear complexes exhibited bands in the fingerprint region which were significantly different from those of the dinuclear complexes. For example, the IR spectrum of dinuclear complex **3a** show peaks at 918, 847, 712, 646 and 473 cm^{-1} which were absent in the IR spectrum of mononuclear complex **3b**. On the other hand **3b** exhibited peaks at 824, 655, 530 and 390 cm^{-1} which were missing in the IR spectrum of **3a**.

Coordination of HMTA to the metal decreases molecular symmetry resulting in a highly complex ^1H NMR spectrum with a multiple spin system making the assignment of the methylene protons difficult. Hence the literature NMR data for the coordinated HMTA or its derivative 1,3,5-triaza-7-phosphaadamantane (PTA) are often reported as a range [1,4,7,52], and a similar strategy is adopted for this study. The proton NMR spectrum of **3a** in acetonitrile-d_3 consists of a sharp singlet at 5.42 ppm integrating for 10 protons, assignable to two identical cyclopentadienyl ligands, while the Cp* analogue, compound **4a,** exhibited a resonance peak integrating for 30 protons and assignable to the two identical pentamethylcyclopentadienyl protons at 1.86 ppm. Multiple resonance peaks assignable to the 12 protons of the methylenes bridging the nitrogen atoms of the HMTA ligand in the dinuclear complexes **3a** and **4a** are observed in the range 4.16–4.50 ppm.

The ^1H NMR spectra of the mononuclear complexes **3b** and **4b** show three resonance peaks each; a singlet peak integrating for 6 protons, assignable to methylene protons adjacent to coordinated nitrogen, and a set of two broad resonance peaks, integrating for 3 protons, each assignable to axial and equatorial protons of methylenes bridging the uncoordinated nitrogen. Similar observations were made by Darensbourg and Daigle in the ^1H NMR spectrum of $Mo(CO)_5$(HMTA) recorded in acetone [53].

In the $^{13}C\{^1H\}$ NMR spectra of the dinuclear complexes **3a** and **4a** (Fig. 1a), a peak corresponding to C2 is observed at ca. 86.6 ppm, shifted downfield as a result of the deshielding effect of the two metal centres. The peak assignable to the less deshielded C6 is observed upfield relative to other methylene carbons at ca. 73 ppm, while the peak corresponding to the four identical methylene carbons C4, C8, C9 and C10 appears at ca. 81.0 ppm. Unlike the dinuclear complexes, the $^{13}C\{^1H\}$ NMR spectra of the mononuclear complexes **3b** and **4b** showed two peaks for the bridging methylene carbons of the coordinated HMTA ligand; one peak corresponding to the three equivalent methylene carbons closer to the coordinated nitrogen and the other peak corresponding to the three equivalent methylenes bridging the uncoordinated nitrogen atoms. The $^{13}C\{^1H\}$ NMR spectrum of **3b** shows a singlet at 83.5 ppm corresponding to the methylene carbons C2, C8 and C9 (Fig. 1b), while a singlet corresponding to the equivalent methylene carbons was observed at 81.8 ppm in the $^{13}C\{^1H\}$ NMR spectrum of compound **4b** indicating a decrease in σ acidity of the metal fragment upon changing from Cp to Cp* which conforms with the expected enhanced π-back donation in Cp* complexes [54]. The peak corresponding to less deshielded methylene carbons C4, C6, and C10 bridging the uncoordinated nitrogen atoms were observed at 71.1 and 71.2 ppm for compounds **3b** and **4b**, respectively, implying that the effect of changing the Cp to Cp* was insignificant on these methylene groups.

Complex **4b** reacted with **1** at room temperature by displacing the $\{Cp^*(CO)_2Fe\}$ fragment to give a mixture of compounds **3a**, **3b**, and $[Cp^*(CO)_2Fe]_2$ rather than the expected mixed ligand complex $[\{Cp(CO)_2Fe\}(\mu\text{-HMTA})\{Fe(CO)_2Cp^*\}](BF_4)_2$. There was no evidence indicating formation of the mixed ligand complex at room temperature. This was probably due to the high electrophilic nature of the $\{Cp(CO)_2Fe\}$ group which rapidly reacted by displacing the relatively less electrophilic $\{Cp^*(CO)_2Fe\}$ group at room temperature. However, when the reaction was repeated and maintained at 0 °C for 1 h the compound $[\{Cp(CO)_2Fe\}(\mu\text{-HMTA})\{Fe(CO)_2Cp^*\}](BF_4)_2$ was obtained as an air-sensitive orange solid which was characterized by NMR spectroscopy.

In another attempt to prepare the mixed ligand complexes, a mixture of a solution of **3b** in acetonitrile and compound **2** in dichloromethane were stirred at room temperature for 3 h after which the starting material **3b** precipitated out as a yellow residue. The acetonitrile complex $[Cp^*(CO)_2Fe(NCMe)]BF_4$ was obtained in 98% yield (based on compound **2**) from the filtrate by precipitation using diethyl ether. The molecular structure, physical and spectroscopic data of $[Cp^*(CO)_2Fe(NCMe)]BF_4$ are reported elsewhere [55]. Thus, the $\{Cp^*(CO)_2Fe\}$ group has preferential binding affinity for NCMe when compared to the coordinated HMTA. It should be noted that based on Pearson's rule on hard and soft acids and bases the preferential binding of the $\{Cp^*(CO)_2Fe\}$ group to acetonitrile does not in any way contradict the formation of the bridged complex **4b**, since the soft acid will interact more strongly with a soft base than a hard base. Generally, metal centres that are electron rich will interact weakly with strong electron-donating ligands. This leads to weak M–L bonding and ease of ligand dissociation. The strong interaction of iron-acetonitrile in $[Cp^*(CO)_2Fe(NCCH_3)]BF_4$ is confirmed by a shorter Fe–N bond (1.924 Å) [55].

To ascertain the water-stability of the reported complexes, the NMR data of the dinuclear HMTA complex **3a** and the mononuclear complex **4b** were also collected in D_2O. These data are given in the Experimental Section. Both the ^1H and ^{13}C NMR spectra did not show any evidence of decomposition. Peaks remained sharp even after allowing the solution to stand for 10 h.

Furthermore, the mass spectroscopy data of compounds **3a** and **4b** collected in 100% water confirmed the stability of these compounds in water. The mass spectrum of **4b** show a base peak at m/z 329 which corresponds to the molecular ion

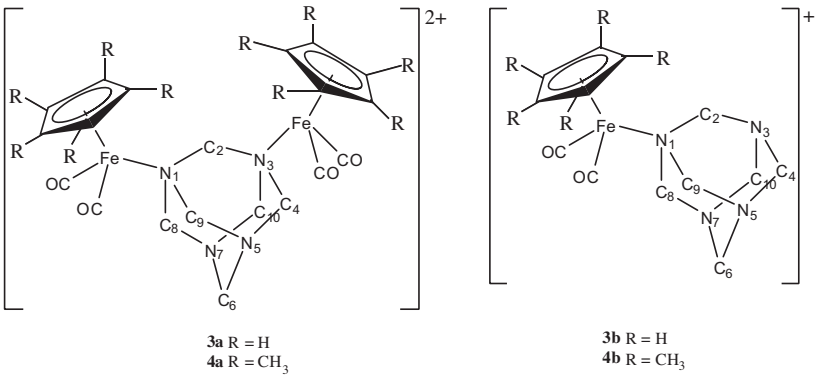

3a R = H
4a R = CH_3

3b R = H
4b R = CH_3

Fig. 1. Atomic numbering scheme of HMTA in dinuclear (a) and mononuclear (b).

Table 1
Selected bond lengths (Å) and angles (°) for $[\{Cp(CO)_2Fe\}_2(\mu\text{-HMTA})](BF_4)_2$ (**3a**).

Bond	Length (Å)	Bonds	Angle (°)
C(8)–N(2)	1.506(3)	N(2)–C(8)–N(1)	112.77(16)
C(8)–N(1)	1.506(3)	N(4)–C(10)–N(1)	112.35(17)
C(9)–N(3)	1.456(3)	C(10)–N(1)–C(9)	107.11(16)
C(9)–N(1)	1.516(3)	C(12)–N(2)–C(11)	106.38(16)
C(10)–N(4)	1.451(3)	C(12)–N(4)–C(10)	110.07(17)
C(10)–N(1)	1.510(3)	C(12)–N(4)–C(13)	109.46(19)
C(13)–N(4)	1.469(3)	C(10)–N(4)–C(13)	109.06(17)
C(13)–N(3)	1.475(3)	C(6)–Fe(1)–C(7)	93.01(11)
N(1)–Fe(1)	2.0858(18)	C(6)–Fe(1)–N(1)	94.48(9)
N(2)–Fe(2)	2.0817(17)	C(7)–Fe(1)–N(1)	95.27(9)

$[Cp^*(CO)_2Fe(HMTA)]^+$, while that of **3a** show a peak of weak intensity at *m*/*z* 317 corresponding to the $[Cp(CO)_2Fe(HMTA)]^+$ fragment. The mass spectra of both compound exhibited fragmentation patterns which mainly involve loss of subsequent carbonyl groups. The full mass spectroscopy data is given in the Experimental Section.

2.1.1. Structural analysis of $[\{Cp(CO)_2Fe\}_2(\mu\text{-HMTA})](BF_4)_2$

The single-crystal X-ray diffraction study reveals that $[\{Cp(CO)_2Fe\}_2(\mu\text{-HMTA})](BF_4)_2$ crystallizes in the orthorhombic $P2_12_12_1$ space group with one dicationic molecule and two counter-anions in the asymmetric unit. The two $\{Cp(CO)_2Fe\}$ units are linked by the HMTA ligand through the nitrogen atoms in which the coordination geometry around Fe can be described as distorted octahedral with three sites occupied by a cyclopentadienyl ligand, while the two carbonyls and the HMTA ligand occupy the remaining three sites. The Fe–N bond distances were found to be 2.0817(17) and 2.0858(18) Å, which are comparable to the 2.092(4) Å in $[(CO)_4Fe(DABCO)$ [30], but longer than the Fe–N bond lengths previously reported for cyclopentadienylirondicarbonyl amine complexes [44,48,50]. The three carbon atoms adjacent to the iron centre form a base with a distorted tetragonal geometry about nitrogen with N–C bonds in the range 1.514 ± 0.010 Å. Valence angles are: Fe–N–C, 111.89 ± 1.51° and C–N–C, 106.94 ± 0.84°. The length of the remaining C–N bonds in the molecule fall in the range 1.458 ± 0.017 Å, unlike the equivalent

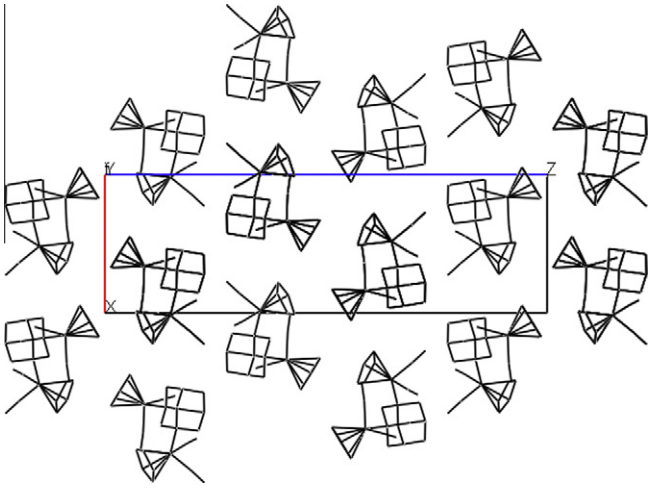

Fig. 3. Crystal packing of compound **3a** viewed down the *b*-axis.

C–N bonds (1.476 Å) reported for the uncoordinated HMTA structure [56]. The difference in bond lengths can be attributed to loss of symmetry upon coordination to the electrophilic iron centre. Similar observations were reported by Hanic and Šubrtová in the structural study of $C_6H_{12}N_4{\cdot}BH_3$ [57] and by Frost et al. in the structural study of PTA·BH_3 [58]. For nitrogen coordinated PTA complexes, elongation of (N)C-N mainly results from alkylation or protonation of PTA, while metallation of PTA results in little or no change in (N)C–N distance [59]. Other selected bond distances and angles of **3a** are listed in Table 1. The ORTEP diagrams showing the atomic numbering scheme and the packing of the molecules in the crystal are shown in Figs. 2 and 3, respectively. Crystallographic and refinement data are given in Table 2.

2.2. Reaction of **3b** and **4b** with $NaBPh_4$

The reaction of mononuclear complexes **3b** and **4b** with $NaBPh_4$ in acetone proceeds smoothly at room temperature with counter-

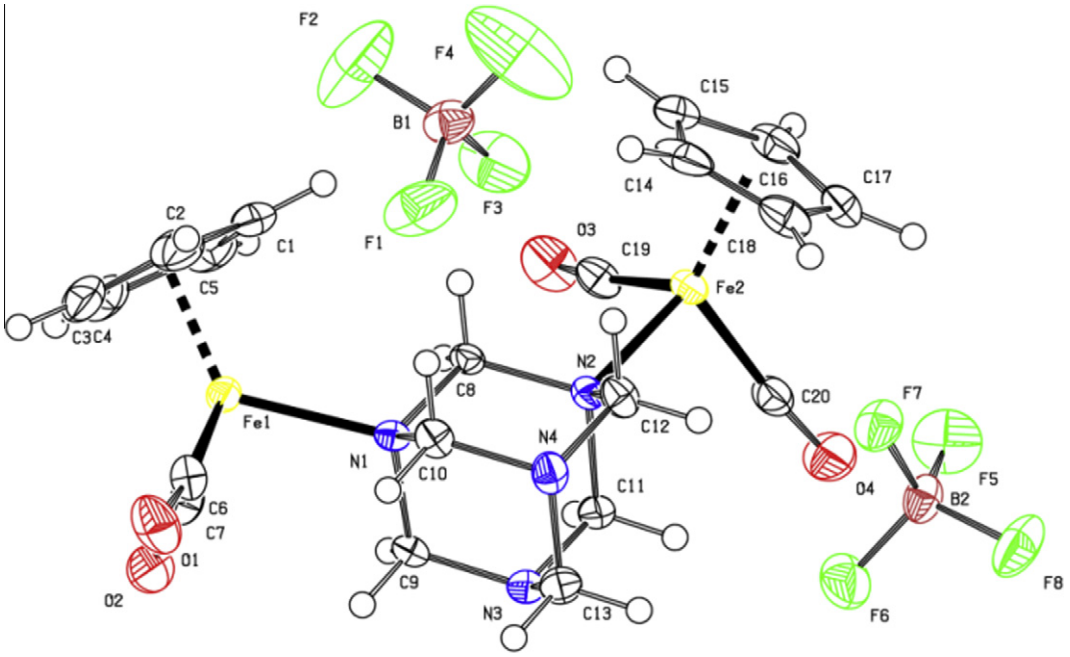

Fig. 2. The molecular structure of **3a** showing atomic numbering scheme. Displacement ellipsoids are drawn at the 50% probability level with H atoms presented as small spheres.

Table 2
Crystal data and structure refinement data for $[\{Cp(CO)_2Fe\}_2(\mu\text{-HMTA})](BF_4)_2$ (**3a**), $[Cp(CO)_2Fe(1\text{-meIm})]BF_4$ (**7**) and $[Cp^*(CO)_2Fe(1\text{-meIm})]BF_4$ (**8**).

Compound	**3a**	**7**	**8**
Empirical formula	$C_{20}H_{22}B_2F_8Fe_2N_4O_4$	$C_{11}H_{11}BF_4FeN_2O_2$	$C_{16}H_{21}BF_4FeN_2O_2$
Formula weight	667.74	345.88	416.01
Temperature (K)	173(2)	173(2)	173(2)
Wavelength (Å)	0.71073	0.71073	0.71073
Crystal system	orthorhombic	monoclinic	orthorhombic
Space group	$P2_12_12_1$	$P2_1/c$	$Pna2_1$
Unit cell dimension			
a (Å)	8.60250(10)	17.8135(6)	17.0840(4)
b (Å)	10.2951(2)	9.9651(4)	13.9877(4)
c (Å)	27.5041(4)	23.9093(10)	7.6884(2)
α (°)	90	90	90
β (°)	90	95.3860(10)	90
γ (°)	90	90	90
Volume (Å^3)	2435.86(7)	4225.5	1839.65(8)
Z	4	12	4
D_{calc} (Mg/m^3)	1.821	1.631	1.502
Absorption coefficient (mm^{-1})	1.29	1.119	0.871
$F(000)$	1344	2088	856
Crystal size (mm)	0.47 × 0.46 × 0.16	0.44 × 0.41 × 0.13	0.44 × 0.40 × 0.01
Crystal description	plate	plate	prism
Crystal colour	brown	yellow	yellow
Theta range for data collection	1.48–27.99°.	1.15–28.00	1.88–28.00
Index ranges			
h	−11 → 11	−23 → 15	−22 → 21
k	−13 → 13	−13 → 9	−18 → 18
l	−36 → 36	−31 → 31	−10 → 10
Reflections collected	33 919	28 785	20 793
Independent reflections	5902	10 195	4441
Internal fit	R(int) = 0.0418	R(int) = 0.0355	R(int) = 0.0465
Absorption correction	integration	integration	integration
Transmission factor (T_{Min}; T_{Max})	0.5823; 0.8202	0.6388; 0.8682	0.7006; 0.9913
Refinement method	full-matrix least-squares on F^2	full-matrix least-squares on F^2	full-matrix least-squares on F^2
Parameters	361	571	241
Goodness-of-fit (GOF) on F^2	1.051	1.046	1.038
Final R indices [$I > 2\sigma(I)$]	R_1 = 0.0284, wR_2 = 0.0705	R_1 = 0.0535, wR_2 = 0.1456	R_1 = 0.0342, wR_2 = 0.0836
R indices (all data)	R_1 = 0.0314, wR_2 = 0.0715	R_1 = 0.0787, wR_2 = 0.1663	R_1 = 0.0418, wR_2 = 0.0870
Largest difference in peak and hole (e Å^{-3})	0.683 and −0.473	1.604 and −0.943	0.400 and −0.312

anion exchange to provide complexes $[Cp(CO)_2Fe(HMTA)]BPh_4$ (**5a**) and $[Cp^*(CO)_2Fe(HMTA)]BPh_4$ (**5b**), respectively. These complexes were obtained in high yields as yellow microcrystalline solids by precipitation using diethyl ether from their CH_2Cl_2 solutions. The bulky BPh_4^- anion renders the cationic complexes soluble in dichloromethane and relatively more soluble in acetone and acetonitrile. It also stabilizes the cations in solution and consequently improves the resolution of their NMR spectra. For example, the ^{1}H NMR spectra of **5a** and **5b** exhibited two doublets corresponding to the axial and equatorial protons of the methylene groups bridging the uncoordinated nitrogen atoms which were observed as broad peaks in the ^{1}H NMR spectra of **3b** and **4b**.

2.3. Reaction of *1* and *2* with DABCO

1,4-Diazabicyclo[2.2.2]octane (DABCO) reacts with one equivalent of the ether complex (**1**) at room temperature to give a mixture of the dinuclear complex $[\{Cp(CO)_2Fe\}_2(\mu\text{-DABCO})](BF_4)_2$ (**6a**) and mononuclear complex $[Cp(CO)_2Fe(DABCO)]BF_4$ (**6b**) in a 9:10 ratio. The reaction of DABCO with two equivalents of compound **1** also gave a mixture of **6a** and **6b**, however, the amount of **6a** in the mixture increased as the amount of compound **1** used in the reaction is increased. The dinuclear complex **6a** formed as an orange precipitate after six hours of reaction and was easily separated by filtration under nitrogen. The mononuclear complex remained in solution and was obtained as a yellow solid by precipitation using diethyl ether. The reaction of DABCO with three equivalents of **1** afforded only the dinuclear complex **6a**. In contrast, the reaction of DABCO with one to three equivalents of the THF complex (**2**) gave only the mononuclear complex $[Cp^*(CO)_2Fe(DABCO)]BF_4$ (**6c**), which was obtained as a yellow solid in low yield by addition of diethyl ether into its solution in CH_2Cl_2. The failure to form the dinuclear complex by $[Cp^*(CO)_2Fe(THF)]BF_4$ can be attributed to the high steric demand of both the $Cp^*(CO)_2Fe$ moiety and the ligand itself. Unlike HMTA, which has a Tolman's cone angle of 118° [60], DABCO has a Tolman's cone angle of *ca.* 132° [61] implying that, once one of its nitrogens is bound to the metal centre, the other nitrogen becomes sterically crowded thus preventing the coordination of the second $Cp^*(CO)_2Fe$ moiety.

Complex **6a** is an air stable orange solid which decomposes without melting at temperatures above 174 °C. It is insoluble in chlorinated solvents and hexane but soluble in water, acetone and acetonitrile. The infrared spectrum of complex **6a** exhibited two bands at 2053 and 2000 cm^{-1} assigned to the ν(CO) of the two equivalent $[Cp(CO)_2Fe]^+$ fragments. Moreover, the ^{1}H NMR spectrum of compound **6a** in D_2O exhibited a singlet at 3.01 ppm assignable to the 12 protons of six equivalent N–CH_2–N groups and presenting a slight downfield shift relative to the N–CH_2–N of free uncoordinated DABCO by 0.34 ppm. A singlet attributed to 10 protons of the two identical η^5-cyclopentadienyl groups appeared at 5.28 ppm. Its $^{13}C\{^1H\}$ NMR spectrum shows three singlets at 58.5, 86.6 and 210.0 ppm assignable to the six identical carbons of the methylene groups, 10 identical carbons of the two η^5-cyclopentadienyl ligands and four identical carbons of the carbonyl groups, respectively, confirming the molecular symmetry of the DABCO bridging the two $[Cp(CO)_2Fe]^+$ fragments. The peak corresponding to methylene carbons of the ligated DABCO also appears downfield relative to the non complexed DABCO ligand (46.7 ppm). This downfield shift can be attributed to the deshielding effect upon the coordination of the DABCO to the elec-

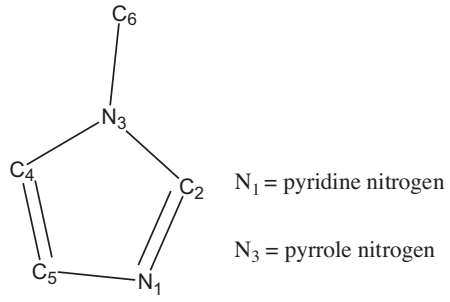

Fig. 4. Diagram of 1-methylimidazole showing the 'pyridine and pyrrole nitrogens'.

trophilic metal centre. These NMR data are in agreement with those reported by Matos and Verkade in their NMR elucidation of the complex [{$(CO)_4Fe$}$_2$(μ-DABCO)] [30].

The mononuclear complexes **6b** and **6c** are moderately air stable and are soluble in water, dichloromethane, acetone and acetonitrile. Each show two strong *ν*(CO) stretching bands, with those of **6c** appearing at lower wavenumbers due to the high electron density at the metal centre. The ^{1}H NMR spectra of **6b** and **6c** exhibit two broad peaks assigned to the two sets of methylene protons. The ^{1}H NMR spectrum of **6b** obtained in D_2O shows a peak corresponding to the six protons of the methylene closer to the coordinated nitrogen at 3.21 ppm, while the peak due to the six protons of the methylenes in the neighbourhood of the uncoordinated nitrogen appeared at 2.84 ppm. Its ^{13}C{^{1}H} NMR spectrum shows two peaks at 58.3 and 46.0 ppm corresponding to carbons bonded to the coordinated nitrogen and those bonded to uncoordinated nitrogen, respectively. The assignment of these peaks was done with the aid of heteronuclear NMR experiments and with comparison of NMR data of the free DABCO ligand. The mass spectrum of the mononuclear compound **6b** recorded in 100% water, showed peaks at *m*/*z* 289, 261 and 233 corresponding to $[Cp(CO)_2Fe(DABCO)]^+$, $[Cp(CO)Fe(DABCO)]^+$ and $[CpFe(DABCO)]^+$, respectively, confirming the stability of the DABCO compounds in water.

Similarly, the ^{1}H NMR spectrum of **6c** obtained in CD_3CN shows peaks corresponding to the two sets of methylene protons at 3.33 and 3.18 ppm. The ^{13}C{^{1}H} NMR spectrum shows two peaks at 56.4 and 44.2 ppm corresponding to carbons bonded to the coordinated nitrogen and those bonded to the uncoordinated nitrogen, respectively.

2.4. Reaction of 1-methylimidazole (1-meIm) with **1** and **2**

Treatment of the etherate complexes **1** and **2** with a slight excess of 1-methylimidazole (1-meIm) in dichloromethane at room temperature furnished the novel iron 1-methylimidazole complexes $[(\eta^5\text{-}C_5R_5)(CO)_2Fe(1\text{-meIm})]BF_4$ (R = H, **7**; and R = CH_3, **8**) in high yields. These complexes and the dimeric iron complexes $[(\eta^5\text{-}C_5R_5)(CO)_2Fe]_2$ were the only products detected in the reaction mixture. The 1-methylimidazole complexes **7** and **8** were obtained as yellow microcrystalline solids by precipitation from their solutions using diethyl ether. Compound **8** exhibited higher stability relative to **7** towards light, air and heat. For instance, the melting point of **8** is significantly higher than that of **7** by *ca.* 100 °C and it was stable in air and exposure to light for several hours in the solid state with minimal degradation. In contrast, compound **7** degraded within 2 h when it was subjected to similar conditions. However, these complexes can be preserved for long periods of time when sealed under nitrogen and kept in the dark at temperatures below 0 °C. The stability of Cp^* complexes is generally enhanced by the more electron-releasing Cp^* ligand. The infrared spectra of compounds **7** and **8** show two strong CO stretching bands as expected. The *ν*(CO) of **8** were as expected lower by *ca.* 13 cm^{-1} as compared to those of **7**.

Two medium absorption bands corresponding to C=C and C=N stretching were observed at *ca.* 1531 and 1515 cm^{-1}, respectively, indicating that the π-electrons of the ring were not involved in coordination. The ^{1}H NMR spectra of compounds **7** and **8** show three peaks corresponding to the protons attached to the three different sp^2 hybridized carbons C2, C4 and C5 (Fig. 4) in the range between 6.89 and 7.90 ppm, which is the typical region for uncoordinated

Table 3
Selected bond lengths (Å) for compounds **7** and –.

7a		**7b**		**7c**		**8**	
Bond	Length (Å)	Bond	Length (Å)	Bond	Length (Å)	Bond	Length (Å)
C(6)–O(1)	1.136(4)	C(17)–O(3)	1.129(5)	C(28)–O(5)	1.136(5)	C(11)–O(1)	1.142(3)
C(6)–Fe(1)	1.787(4)	C(17)–Fe(2)	1.787(4)	C(28)–Fe(3)	1.788(4)	C(11)–Fe(1)	1.778(3)
C(7)–O(2)	1.136(5)	C(18)–O(4)	1.139(5)	C(29)–O(6)	1.133(4)	C(12)–O(2)	1.133(3)
C(7)–Fe(1)	1.789(4)	C(18)–Fe(2)	1.788(4)	C(29)–Fe(3)	1.789(4)	C(12)–Fe(1)	1.787(3)
C(8)–C(9)	1.357(5)	C(19)–C(20)	1.352(6)	C(30)–C(31)	1.354(5)	C(13)–N(1)	1.330(3)
C(8)–N(1)	1.385(5)	C(19)–N(3)	1.376(5)	C(30)–N(5)	1.380(4)	C(13)–N(2)	1.347(3)
C(9)–N(2)	1.372(5)	C(20)–N(4)	1.365(5)	C(31)–N(6)	1.367(5)	C(14)–C(15)	1.362(3)
C(10)–N(1)	1.326(4)	C(21)–N(3)	1.318(4)	C(32)–N(5)	1.328(4)	C(14)–N(1)	1.385(3)
C(10)–N(2)	1.339(4)	C(21)–N(4)	1.336(4)	C(32)–N(6)	1.341(4)	C(15)–N(2)	1.362(3)
N(1)–Fe(1)	1.973(3)	N(3)–Fe(2)	1.977(3)	N(5)–Fe(3)	1.980(3)	N(1)–Fe(1)	1.9781(18)

Table 4
Selected bond angles (°) for compounds **7** and **8**.

7a		**7b**		**7c**		**8**	
Bonds	Angle (°)	Bonds	Angle (°)	Bonds	Angle (°)	Bonds	Angle (°)
N(1)–C(10)–N(2)	111.0(3)	N(3)–C(21)–N(4)	110.7(3)	N(5)–C(32)–N(6)	110.2(3)	N(1)–C(13)–N(2)	110.6(2)
C(9)–C(8)–N(1)	108.8(3)	C(20)–C(19)–N(3)	108.6(4)	C(31)–C(30)–N(5)	108.3(3)	C(15)–C(14)–N(1)	108.9(2)
C(8)–C(9)–N(2)	106.6(3)	C(19)–C(20)–N(4)	106.7(3)	C(30)–C(31)–N(6)	107.0(3)	C(14)–C(15)–N(2)	106.71(19)
C(10)–N(1)–C(8)	106.0(3)	C(21)–N(3)–C(19)	106.3(3)	C(32)–N(5)–C(30)	106.7(3)	C(13)–N(1)–C(14)	105.91(19)
C(10)–N(2)–C(9)	107.6(3)	C(21)–N(4)–C(20)	107.6(3)	C(32)–N(6)–C(31)	107.7(3)	C(13)–N(2)–C(15)	107.88(19)
C(6)–Fe(1)–C(7)	93.00(17)	C(17)–Fe(2)–C(18)	92.31(18)	C(28)–Fe(3)–C(29)	95.72(18)	C(11)–Fe(1)–C(12)	93.55(13)
C(6)–Fe(1)–N(1)	93.27(14)	C(17)–Fe(2)–N(3)	93.09(14)	C(28)–Fe(3)–N(5)	91.11(14)	C(11)–Fe(1)–N(1)	94.72(10)
C(7)–Fe(1)–N(1)	93.73(14)	C(18)–Fe(2)–N(3)	95.92(15)	C(29)–Fe(3)–N(5)	92.79(14)	C(12)–Fe(1)–N(1)	93.04(10)

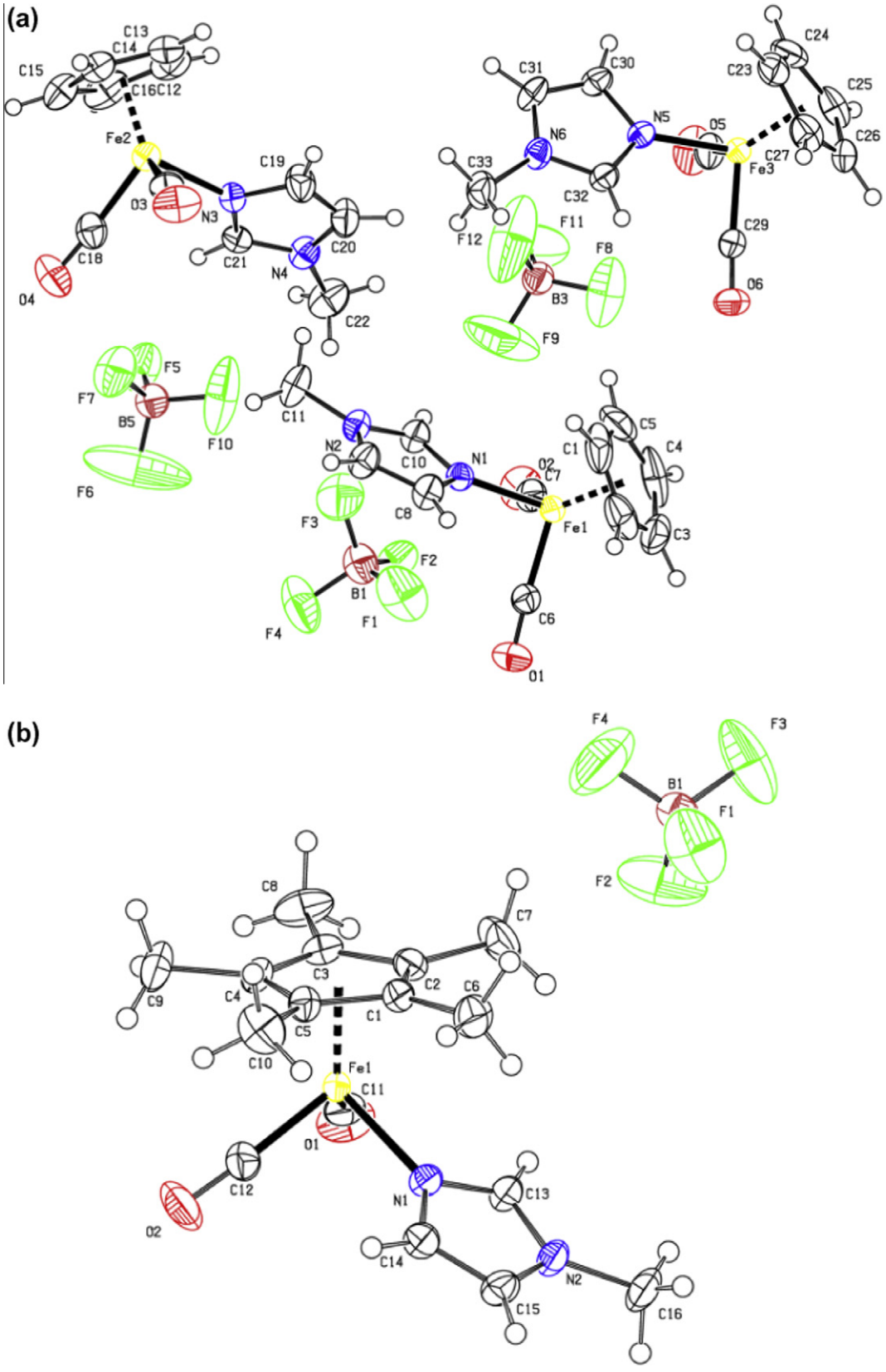

Fig. 5. The molecular structures of **7** (a) and **8** (b) showing atomic numbering scheme. Displacement ellipsoids are drawn at the 50% probability level with H atoms presented as small spheres.

olefins. This supports the IR data and is supported by the single crystal X-ray diffraction data presented in Table 3. Peaks corresponding to the protons attached to C5 and C2 appear at *ca.* 7.23 and 7.88 ppm, respectively, which is a downfield shift of *ca.* 0.16 and 0.31 ppm relative to the uncoordinated 1-methylimidazole ligand. The coordination of the 1-methylimidazole is via the 'pyridine nitrogen' and this

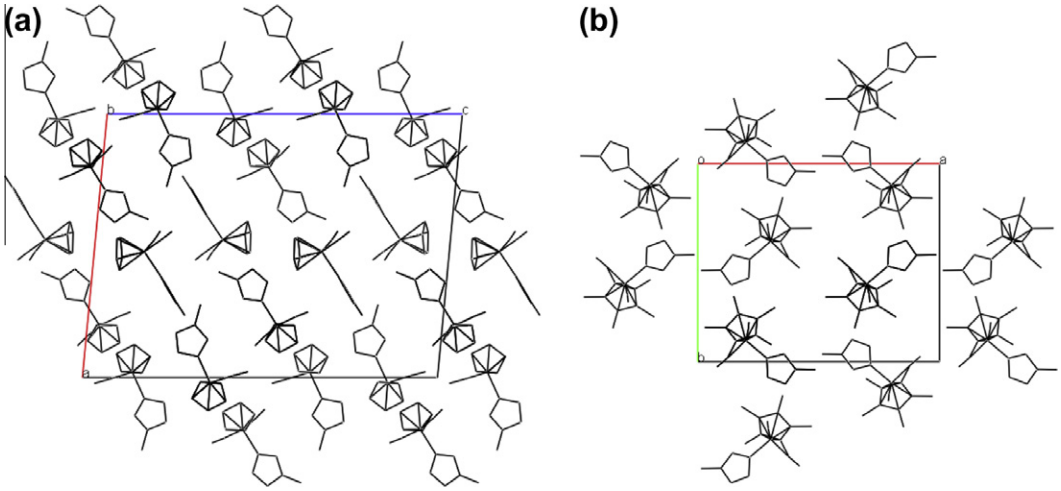

Fig. 6. (a) Crystal packing of **7** viewed down the *b*-axis. (b) Crystal packing of **8** viewed down the *c*-axis.

has the effect of deshielding the neighbouring carbons C5 and C2. The effect appears to diminish across the ring, implying that the delocalized π-electrons are not evenly distributed within the ring of the coordinated 1-methylimidazole and hence the geometry of the imidazole ring is slightly affected. This is clearly reflected in the single crystal X-ray diffraction data presented in Table 3. $^{13}C\{^1H\}$ NMR spectra of compounds **7** and **8** show a slight downfield shift of all peaks relative to the free 1-methyimidazole ligand with a larger downfield shift observed for **7** than for **8**. The NMR data of compounds **7** and **8** collected in D_2O were similar to those collected in CD_3OD and did not show any evidence of decomposition even after 37 h. The mass spectrum of compound **8** collected in 100% water showed a peak at *m*/*z* 329 corresponding to the molecular ion $[Cp^*(CO)_2Fe(1\text{-meIm})]^+$, further confirming the stability of 1-methylimidazole complexes in water.

*2.5. Structural analysis of $[(\eta^5\text{-}C_5R_5)(CO)_2Fe(1\text{-meIm})]BF4$ (R = H, CH_3) (**7** and **8**)*

For a more detailed understanding of the bonding of the 1-methylimidazole (1-meIm) ligand, the molecular structures of $[Cp(CO)_2Fe(1\text{-meIm})]BF_4$ (**7**) and $[Cp^*(CO)_2Fe(1\text{-meIm})]BF_4$ (**8**) were studied by single crystal X-ray crystallography. Selected bond distances and angles are given in Tables 3 and 4, respectively. Crystals of compound **7** were obtained as yellow plates that crystallized in the monoclinic $P2_1/c$ space group, with three independent molecular cations and anions each in the asymmetric unit, while compound **8** crystallized in the orthorhombic *Pna*21 space group as yellow prisms, with one cation and a counterion in the asymmetric unit. Crystal data and structure refinement information for compounds **3a**, **7** and **8**, are summarized in Table 2. The 1-methylimidazole ligand is σ-bonded to iron via the 'pyridine nitrogen' through the lone pair of electrons in the hybrid orbital. This mode of bonding is thermodynamically favoured in order to retain the aromaticity within the imidazole ring [62]. The coordination about the iron is the familiar 3-legged piano-stool geometry adopted by the $[(\eta^5\text{-}C_5R_5)(CO)_2Fe(1\text{-meIm}]^+$ (Fig. 5a and b) with mean bond angles around Fe involving the basal carbonyl and imidazole ligands of about 90°.

The Fe–N bond lengths are between 1.973(3) and 1.9781(18) Å as expected for iron-cyclic amine complexes [63–65]. These values are close to Fe–N = 1.970(7) Å in the iron benzimidazole complex $[Cp(CO)_2Fe(C_7H_6N_2)]BPh_4$ [35], Fe–N = 1.983(28), 1.973(31) Å observed in the two independent molecules of $[Cp(CO)_2Fe(C_5H_5N)]SbF_6$ [65] and falls within the range (1.958(5)–1.999(2) Å) reported for iron imidazole complexes [36,66,67]. The Fe–N bond (1.977 Å) in **7** is marginally shorter than the average Fe–N bond (1.978 Å) in **8** (Table 3). This was expected because the Cp^* ligand is known to increase electron density on the metal centre which in this case leads to a weaker Fe–N bond in **8** relative to that observed in the Cp analogue. 1-methylimidazole is planar and lies on the same plane with Fe, with angles about the 'pyridine nitrogen' adding up to *ca.* 360 °C. The 1-methylimidazole geometry is similar to that of the coordinated 1-methylimidazole in $[Fe(TPP)(1\text{-meIm})N_3]$ [67] and bis(1-methylimidazole) complexes of manganese [68].

Fig. 6a and b shows the packing of **7** and **8**, respectively, in the crystal lattice. The packing of **7** is characterized by an inversion centre resulting in a head to head and tail to tail orientation of the molecules in alternating layers. On the other hand in **8** discrete cationic moieties are separated by alternating BF_4^- anions arranged in layers forming a zigzag pattern that are related by glide planes perpendicular to the (0,1,0) and (1,0,0) axes and a 2-fold screw axis along the *z*-axis.

3. Conclusion

The ether complexes, $[(\eta^5\text{-}C_5R_5)(CO)_2Fe(E)]BF_4$ (R = H; E = Et_2O and R = CH_3, E = THF) have been shown to undergo nucleophilic substitution with N-heterocyclic ligands such as hexamethylenetetramine (HMTA), 1,4-diazabicyclo[2.2.2]octane (DABCO) and 1-methylimidazole (1-meIm) to form dinuclear and mononuclear complexes of the types $[\{(\eta^5\text{-}C_5R_5)(CO)_2Fe\}_2L](BF_4)_2$ (R = H; L = HMTA, DABCO; R = CH_3; L = HMTA) and $[(\eta^5\text{-}C_5R_5)(CO)_2FeL]BF_4$ (L = HMTA, DABCO, 1-meIm), respectively. The more electrophilic Cp containing metal fragment $[Cp(CO)_2Fe]^+$ displaced the Cp^* analogue $[Cp^*(CO)_2Fe]^+$ from its complex with HMTA when the reaction was carried out at room temperature, but not when the reaction was conducted at 0 °C. The reaction of the ethereal complexes with 1-methylimidazole gave complexes of the type $[(\eta^5\text{-}C_5R_5)(CO)_2Fe(1\text{-meIm})]BF_4$ (R = H, CH_3). The NMR, IR and single crystal X-ray diffraction data of the compounds $[Cp^*(CO)_2Fe(1\text{-meIm})]BF_4$ and $[Cp(CO)_2Fe(1\text{-meIm})]BF_4$ show that the iron centre has preferential binding affinity towards the 'pyridine nitrogen' of the 1-methylimidazole ring resulting in a positive inductive effect that makes the Fe–N bond in 1-methylimidazole complexes significantly shorter than the Fe–N bond in the dinuclear HMTA complex.

4. Experimental

4.1. General

All manipulations were carried out under nitrogen atmosphere using Schlenk line techniques. Nitrogen (Afrox) was dried over phosphorus(V) oxide. Reagent grade THF, hexane and Et_2O were distilled from sodium/benzophenone and stored over sodium wire; CH_2Cl_2 was distilled from phosphorus(V) oxide and used immediately. Acetone and MeCN were distilled from anhydrous $CaCl_2$ and stored over type 4A molecular sieves. The other chemical reagents were obtained from the suppliers shown in parentheses: dicyclopentadiene, 1,2,3,4,5-pentamethylcyclopentadiene, iron pentacarbonyl, tetrafluoroboric acid diethyl ether, iodomethane, mercury (Aldrich), silver tetrafluoroborate and DABCO (Merck), HMTA (BDH), sodium (Fluka) and iodine (Unilab) were used as supplied. Melting points were recorded on an Ernst Leitz Wetzlar hot-stage microscope and are uncorrected. Elemental analyses were performed on a LECO CHNS-932 elemental analyzer. Infrared spectra were recorded using an ATR PerkinElmer Spectrum 100 spectrophotometer between 4000 and 400 cm^{-1}, in the solid state. Mass spectra were recorded on an Agilent 1100 series LC/MSD trap with an electrospray ionization (ESI) source and quadrupole ion trap mass analyzer by direct infusion and ESI operated in the positive mode. Deionised water (100%) was used as mobile phase and 10 μl of the sample injected at a 0.3 ml/min flow rate. NMR spectra were recorded on Bruker topspin 400 MHz and 600 MHz spectrometers and the chemical shifts are reported in ppm. The deuterated solvents, D_2O (Aldrich, 99.9%), $CDCl_3$ (Aldrich, 99.8%), acetone-d_6 (Aldrich, 99.5%), and acetonitrile-d_3 (Aldrich, 99.8%), were used as purchased. The precursors $[CpFe(CO)_2(OEt_2)]BF_4$ [44] and $[Cp^*(CO)_2Fe(THF)]BF_4$ [69] were prepared as previously reported.

4.2. Preparation of $[\{Cp(CO)_2Fe\}_2(\mu\text{-HMTA})](BF4)_2$, **3a**

A solution of HMTA (0.219 g, 1.56 mmol) in CH_2Cl_2 (20 ml) was added to a solution of the ether complex **1** (2.200 g, 6.51 mmol) in CH_2Cl_2 (20 ml) in a Schlenk tube and the mixture was stirred for 10 h under nitrogen at room temperature after which an orange precipitate formed. The red mother liquor was syringed off and the precipitate washed with portions of CH_2Cl_2 (5 × 10 ml), and dried under reduced pressure resulting in an orange powdery solid of **3a**. Yield: 1.012 g, 97%. *Anal.* Calc. for $C_{20}H_{22}B_2F_8Fe_2N_4O_4$: C, 35.93; H, 3.29; N, 8.38. Found: C, 36.03; H, 3.27; N, 8.22%. ^1H NMR (400 MHz, CD_3CN): δ 5.42 (s, 10H, C_5H_5), 4.16 (s, 2H, CH_2), 4.38–4.47 (m, 8H, CH_2), 4.50(s, 2H, CH_2). $^{13}C\{^1H\}$ NMR (400 MHz, CD_3CN): δ 86.37 (C_5H_5), 86.77 (C2), 80.17 (C4, C8, C9, C10), 68.47 (C6), 208.63 (CO). ^1H NMR (600 MHz, D_2O): δ 5.47 (s, 10H, C_5H_5), 4.32–4.86 (m, 12H, CH_2). $^{13}C\{^1H\}$ NMR (600 MHz, D_2O): δ 86.38 (C_5H_5), 86.72 (C2), 79.71 (C4, C8, C9, C10), 68.62 (C6), 208.94 (CO). Ms (ESI, water 100%, 350 °C) *m*/*z* (%) 317 (13) $[Cp(CO)_2Fe(HMTA)]^+$, 261 (100) $[CpFe(HMTA)]^+$. IR (solid state): ν(CO) 2058, 2009 cm^{-1}. Decomposes at temperature >196 °C.

4.3. Preparation of $[Cp(CO)_2Fe(HMTA)]BF_4$, **3b**

A Schlenk tube equipped with a magnetic stirrer was charged with a solution of compound **1** (0.580 g, 1.72 mmol) in CH_2Cl_2 (10 ml) in the dark and a solution of HMTA (0.300 g, 2.14 mmol) in CH_2Cl_2 (20 ml) added. The mixture was stirred at room temperature for 16 h after which a yellow precipitate formed. The mixture was then filtered through a cannula and the residue washed with portions of CH_2Cl_2 (3 × 10 ml) and the residue dried under reduced pressure to give a yellow solid of **3b**. Yield: 0.65 g, 94%. *Anal.* Calc. for $C_{13}H_{17}BF_4FeN_4O_2$: C, 38.61; H, 4.21; N, 13.86. Found: C, 38.60; H, 4.15; N, 13.76%. ^1H NMR (600 MHz, CD_3CN): δ 5.39 (s, 5H, C_5H_5), 4.83 (br. s, 3H, axial), 4.46 (br s, 3H, equitorial), 4.60 (br, s 6H, CH_2). $^{13}C\{^1H\}$ NMR (600 MHz, CD_3CN): δ 86.37 (C_5H_5), 83.49 (C2, C8, C9), 71.06 (C4, C6, C10), 209.79 (CO). IR (solid state): ν(CO) 2054, 2003 cm^{-1}. Decomposes at temperature >183 °C.

4.4. Preparation of $[Cp(CO)_2Fe(HMTA)]BPh_4$, **5a**

Into a solution of $[Cp(CO)_2Fe(HMTA)]BF_4$ (0.120 g, 0.30 mmol) in acetone (10 ml), a solution of $NaBPh_4$ (0.180 g, 0.53 mmol) in acetone (15 ml) was added and the mixture stirred for 4 h. The solvent was removed under reduced pressure and the residue extracted with CH_2Cl_2 (15 ml). Diethyl ether was added to the extract until the yellow precipitate had formed. The mixture was allowed to stand for 20 min after which the mother liquor was syringed off. The residue was washed with diethyl ether (2 × 5 ml) and then dried under reduced pressure to give 0.17 g (90% yield) of a yellow solid (**5a**). *Anal.* Calc. for $C_{37}H_{37}BFeN_4O_2$: C, 69.81; H, 5.82; N, 8.81. Found: C, 70.24; H, 5.26; N, 8.95%.^1H NMR (400 MHz, acetone-d_6): δ 5.69 (s, 5H, C_5H_5), 4.87 (s, 6H, $(CH_2)_3$), 4.74 (d, J_{HH} = 12.29, 3H, axial CH), 4.56(d, J_{HH} = 12.13, 3H, equatorial CH). $^{13}C\{^1H\}$ NMR (400 MHz, acetone-d_6): δ 87.89 (C_5H_5), 86.89 (C2, C8, C9), 72.47 (C4, C6, C10). IR (solid state): ν(CO) 2052, 2004 cm^{-1}. M.p., 138–139 °C.

4.5. Reaction of DABCO with one equivalent of $[Cp(CO)_2Fe(OEt_2)]BF_4$

A solution of complex **1** (0.940 g, 2.78 mmol) in CH_2Cl_2 (15 ml) and DABCO (0.300 g, 2.68 mmol) in CH_2Cl_2 (10 ml) was stirred at room temperature overnight after which a yellow precipitate formed. This was filtered via a cannula and the residue washed with CH_2Cl_2 (5 × 10 ml) to give 0.77 g (45% yield) of a yellow solid (**6a**). *Anal.* Calc. for $C_{20}H_{22}B_2F_8Fe_2N_2O_4$: C, 37.50; H, 3.44; N, 4.38. Found: C, 37.29; H, 3.60; N, 4.67%. ^1H NMR (400 MHz, CD_3CN): δ 5.33 (s, 5H, C_5H_5), 3.00 (s, 12H, CH_2), $^{13}C\{^1H\}$ NMR (400 MHz, CD_3CN): δ 86.70 (C_5H_5), 58.21 (CH_2), 209.79 (CO). ^1H NMR (600 MHz, D_2O): δ 5.28 (s, 5H, C_5H_5), 3.01 (s, 12H, CH_2), $^{13}C\{^1H\}$ NMR (600 MHz, D_2O): δ 86.63 (C_5H_5), 58.52 (CH_2), 210.02 (CO). IR (solid state): ν(CO) 2053, 2000 cm^{-1}. Decomposes at temperature >174 °C.

The filtrate was treated as follows: diethyl ether was added and the mixture allowed to stand for 2 h when a yellow precipitate formed. The mother liquor was syringed off and the precipitate washed with 3 × 10 ml of diethyl ether to give 0.54 g (52% yield) of a yellow solid (**6b**). *Anal.* Calc. for $C_{13}H_{17}BF_4FeN_2O_2$: C, 41.49; H, 4.52; N, 7.45. Found: C, 41.98; H, 4.77; N, 7.37%. ^1H NMR (600 MHz, D_2O): δ 5.39 (s, 5H, C_5H_5), 3.14 (CH_2), 2.84 (CH_2). $^{13}C\{^1H\}$ NMR (600 MHz, D_2O); δ 86.75 (C_5H_5), 58.31 (CH_2) 46.00 (CH_2) 210.60 (CO). Ms (ESI, water 100%, 350 °C) *m*/*z* (%) 289 (21) $[Cp(CO)_2Fe(DABCO)]^+$, 233 (100) $[CpFe(DABCO)]^+$, 113 (15) [DABCO + H]. IR (solid state): ν(CO) 2050, 1996 cm^{-1}.

4.6. Reaction of DABCO with three equivalent of $[Cp(CO)_2Fe(OEt_2)]BF_4$

A Schlenk tube was charged with a solution of complex **1** (1.921 g, 5.68 mmol) in CH_2Cl_2 (15 ml) and a solution of DABCO (0.212 g, 1.89 mmol) in CH_2Cl_2 (10 ml) added. The mixture was stirred for 6 h at room temperature after which an orange precipitate formed. The mother liquor was removed by filtration using a cannula and the residue washed with CH_2Cl_2 (3 × 5 ml) and dried under reduced pressure, resulting in an orange solid. The residue was purified further by recrystallization from acetone/diethyl ether and dried under reduced pressure to give a yellow solid of **6a**. Yield: 0.860 g, 71%. *Anal.* Calc. for $C_{20}H_{22}B_2F_8Fe_2N_2O_4$: C, 37.50; H, 3.44; N, 4.38. Found: C, 37.20; H, 3.23; N, 4.12%. ^1H NMR (400 MHz, CD_3CN): δ 5.33 (s, 5H, C_5H_5), 3.00 (s, 12H, CH_2), $^{13}C\{^1H\}$ NMR (400 MHz, CD_3CN): δ 86.70 (C_5H_5), 58.21 (CH_2),

209.79 (CO). IR (solid state): ν(CO) 2053, 2000 cm^{-1}. Decomposes at temperature >174 °C.

4.7. Preparation of $[Cp^*(CO)_2Fe(DABCO)]BF_4$, **6c**

A solution mixture of complex **2** (0.300 g, 0.74 mmol) in CH_2Cl_2 (15 ml) and DABCO (0.030 g, 0.27 mmol) in CH_2Cl_2 (10 ml) was stirred at room temperature overnight. Diethyl ether (30 ml) was added to the mixture and the mixture then allowed to stand undisturbed for 16 h at room temperature. A yellow microcrystalline solid collected on the walls of Schlenk tube. The mother liquor was syringed off, the crystals were washed with diethyl ether (2 x 5 ml) and dried under reduced pressure to give 0.03 g (25% yield) of yellow solid, **6c**. *Anal.* Calc. for $C_{18}H_{27}BF_4FeN_2O_2$: C, 48.43; H, 6.05; N, 6.28. Found: C, 48.87; H, 6.14; N, 5.77%. ^{1}H NMR (400 MHz, CD_3CN): δ 2.01 (s, 15H, $C_5(CH_3)_5$), 3.17 (t, J_{HH} = 6.68 Hz, 6H, CH_2), 3.34 (t, J_{HH} = 6.74, 6H, $(CH_2)_3$). $^{13}C\{^1H\}$ NMR (400 MHz, CD_3CN): δ 8.75 ($C_5(CH_3)_5$), 44.17 (CH_2), 51. 11 (CH2) 97.88 ($\underline{C}_5(CH_3)_5$) 212.41 (CO). IR (solid state): ν(CO) 2021, 1969 cm^{-1}.

4.8. Preparation of $[\{Cp^*(CO)_2Fe\}_2(\mu\text{-HMTA})](BF_4)_2$, **4a**

A solution of HMTA (0.142 g, 1.01 mmol) in CH_2CH_2 (10 ml) was added dropwise into a stirred solution of compound **2** (1.650 g, 4.06 mmol) in CH_2Cl_2 (10 ml) within 60 s. The mixture was stirred under nitrogen at room temperature overnight and then filtered into a pre-weighed Schlenk tube. Diethyl ether was added until an orange precipitate formed and the mixture was allowed to stand for 30 min, after which the mother liquor was syringed off. The residue was washed with portions of diethyl ether (3 × 10 ml) and dried under reduced pressure to give the orange solid of **4a**. Yield: 0.275 g, 34%. *Anal.* Calc. for $C_{30}H_{42}B_2F_8Fe_2N_4O_4$: C, 44.55; H, 5.20; N, 6.93. Found: C, 44.34; H, 5.35; N, 6.88%. ^{1}H NMR (400 MHz, CD_3CN): δ 1.86 (s, 30H, $C_5(CH_3)_5$), 4.32–4.50 (m, 12H, $(CH_2)_6$), $^{13}C\{^1H\}$ NMR (400 MHz, CD_3CN): δ 8.93 ($C_5(\underline{C}H_3)_5$), 86.43 (C2), 81.90 (C4,C8, C9,C10), 78.42(C6), 98.45 ($\underline{C}_5(CH_3)_5$), 211.76 (CO). IR (solid state): ν(CO) 2035, 1991 cm^{-1}.

4.9. Preparation of $[Cp^*(CO)_2Fe(HMTA)]BF_4$, **4b**

A Schlenk tube was charged with a solution of compound **2** (0.633 g, 1.55 mmol) in CH_2Cl_2 (15 ml) and a solution of HMTA (0.250 g, 1.79 mmol) in CH_2Cl_2 (20 ml) was added. The mixture was stirred at room temperature under nitrogen for 18 h. The mixture was then filtered through a cannula into a pre-weighed Schlenk tube and diethyl ether was then added until a yellow precipitate formed. This was allowed to stand for 10 min after which the mother liquor was removed by filtration and the yellow residue washed with portions of CH_2Cl_2 (4 × 10 ml) and dried under reduced pressure. Yield: 0.45 g, 61%. *Anal.* Calc. for $C_{18}H_{27}BF_4FeN_4O_2$: C, 45.57; H, 5.70; N, 11.81. Found: C, 46.01; H, 5.86; N, 11.74%. ^{1}H NMR (400 MHz, CD_3CN): δ 1.83 (s, 15H, $C_5(CH_3)_5$), 4.84 (br. s, 6H,$(CH_2)_3$), 4.49 (br, s, 6H, $(CH_2)_3$). $^{13}C\{^1H\}$ NMR (400 MHz, CD_3CN): δ 8.39 ($C_5(\underline{C}H_3)_5$), 71.25 (C4, C6, C10), 81.84 (C2, C8, C9), 98.98 ($\underline{C}_5(CH_3)_5$). 210.51 (CO). ^{1}H NMR (600 MHz, D_2O): δ 1.85 (s, 15H, $C_5(CH_3)_5$), 4.59 (br. s, 6H,$(CH_2)_3$), 4.53 (br, s, 6H, $(CH_2)_3$). $^{13}C\{^1H\}$ NMR (600 MHz, D_2O): δ 8.98 ($C_5(\underline{C}H_3)_5$), 71.72 (C4, C6, C10), 80.24 (C2, C8, C9), 98.75 ($\underline{C}_5(CH_3)_5$). 211.84 (CO). Ms(ESI, water 100%, 350 °C) m/z (%) 387 (100) $[Cp^*(CO)_2Fe(HMTA)]^+$, 359 (12) $[Cp^*(CO)Fe(HMTA)]^+$, 331 (28) $[Cp^*Fe(HMTA)]^+$. IR (solid state): ν(CO) 2031, 1982 cm^{-1}. M.p., 159–161 °C.

4.10. Preparation of $[Cp^*(CO)_2Fe(HMTA)]BPh_4$, **5b**

The solution of **4b** (0.090 g, 0.19 mmol) in acetone was treated with a solution of $NaBPh_4$ (0.100 g, 0.29 mmol) in acetone (15 ml) and the rest of the procedure was executed as described in Section 4.4 to give 0.11 g (82%) of compound **5b**. *Anal.* Calc. for $C_{42}H_{47}BFeN_4O_2$: C, 71.39; H, 6.66; N, 7.93. Found: C, 70.72; H, 6.70; N, 8.17%. ^{1}H NMR (400 MHz, acetone-d_6): δ 2.01 (s, 15H, $C_5(CH_3)_5$), 4.68 (s, 6H, CH_2), 4.60 (s, 3H, axial, CH), 4.57 (s, 3H, equatorial CH), 6.77 (br, 4H, *p*-CH), 6.92 (br, 8H, *o*-CH), 7.33 (br, 8H, *m*-CH). $^{13}C\{^1H\}$ NMR (400 MHz, acetone-d_6): δ 10.02 ($C_5(CH_3)_5$), 72.67 (C4, C6, C10), 83.29 (C2, C8, C9), 99.50 ($\underline{C}_5(CH_3)_5$), 122.22 (*para*-C, Ph), 125.97 (*meta*-C, Ph), 130.90 (B-C)137.05 (*ortho*-C, Ph). IR (solid state): ν(CO) 2029, 1986 cm^{-1}. M.p., 149–150 °C.

4.11. Preparation of $[Cp(CO)_2Fe(1\text{-meIm})]BF_4$, **7**

1-Methylimidazole (0.40 ml, 5.04 mmol) was added to a solution of compound **1** (0.532 g, 1.57 mmol) in CH_2Cl_2 (10 ml) in a Schlenk tube and the mixture stirred under nitrogen at room temperature for 6 h. Into the resultant yellow-brown solution diethyl ether was added until a yellow precipitate was formed. The precipitate was allowed to stand for 5 min after which the mother liquor was syringed off and the yellow residue was washed with diethyl ether (3 × 5 ml). Drying of the residue under reduced pressure for 5 h gave 0.489 g (90%) of compound **7**. *Anal.* Calc. for $C_{11}H_{11}BF_4FeN_2O_2$: C, 38.15; H, 3.18; N, 8.09. Found: C, 37.90; H, 3.25; N, 8.16%. ^{1}H NMR (400 MHz, MeOD): δ 7.85 (s, 1H, CH), 7.19 (s, 1H, CH), 6.93 (s, 1H, CH), 5.38 (s, 5H, C_5H_5), 3.71 (s, 3H, CH_3), $^{13}C\{^1H\}$ NMR (400 MHz, MeOD): δ 87.90 (C_5H_5), 36.08 (CH_3), 125.19 (CH), 136.08 (CH), 209.79 (CO). ^{1}H NMR (600 MHz, D_2O): δ 7.70 (s, 1H, CH), 7.06 (s, 1H, CH), 6.86 (s, 1H, CH), 5.28 (s, 5H, C_5H_5), 3.62 (s, 3H, CH_3), $^{13}C\{^1H\}$ NMR (600 MHz, D_2O): δ 86.35 (C_5H_5), 34.10 (CH_3), 123.56 (CH), 134.62 (CH), 211.34 (CO). IR (solid state): ν(CO) 2052, 2000 cm^{-1}. M.p., 48–50 °C.

4.12. Reaction of $[Cp^*(CO)_2Fe(1\text{-meIm})]BF_4$, **8**

Into a solution of $[Cp^*(CO)_2Fe(THF)]BF_4$ (0.370 g, 0.91 mmol) in CH_2Cl_2 (15 ml) 1-methylimidazole (0.30 ml, 3.78 mmol) was added and the mixture stirred in the dark for 8 h at room temperature. After this period the reaction mixture changed colour from red to yellow. It was then filtered into a pre-weighed Schlenk tube and diethyl ether (30 ml) was added into the filtrate. The mixture was allowed to stand for 10 min after which a bright yellow crystalline solid formed. The mother liquor was syringed off and the residue was washed with portions of diethyl ether (2 × 10 ml), and then dried under reduced pressure. Yield: 0.364 g, 96% of **8**. *Anal.* Calc. for $C_{16}H_{21}BF_4FeN_2O_2$: C, 46.15; H, 5.04; N, 6.73. Found: C, 46.11; H, 5.20; N, 6.65%. ^{1}H NMR (400 MHz, CD_3OD): δ 1.78 (s, 15H, $C_5(CH_3)_5$), 3.76 (s, 3H, N–CH_3), 6.89 (s, 1H, =CH), 7.25 (s, 1H, =CH), 7.90 (s, 1H, =CH), $^{13}C\{^1H\}$ NMR (400 MHz, $CDCl_3$): δ 9.32 ($C_5(\underline{C}H_3)_5$), 35.12 (N-CH_3), 98.36 ($\underline{C}_5(CH_3)_5$), 123.60 (=CH), 132.55 (=CH), 212.42 (CO). ^{1}H NMR (400 MHz, D_2O): δ 1.68 (s, 15H, $C_5(CH_3)_5$), 3.64 (s, 3H, N–CH_3), 6.80 (s, 1H, =CH), 7.07 (s, 1H, =CH), 7.69 (s, 1H, =CH), $^{13}C\{^1H\}$ NMR (600 MHz, D_2O): δ 8.37 ($C_5(\underline{C}H_3)_5$), 34.02 (N–CH_3), 98.38 ($\underline{C}_5(CH_3)_5$), 123.66 (=CH), 133.13 (=CH), 213.33 (CO). Ms (ESI, water 100%, 350 °C) m/z (%) 329 (30) $[Cp^*(CO)_2Fe(1\text{-meIm})]^+$, 305 (28) $[Cp^*(CO)Fe(1\text{-meIm})+2H_2]^+$, 273 (100) $[Cp^*Fe(1\text{-meIm})]^+$. IR (solid state): ν(CO) 2041, 1986 cm^{-1}. M.p, 145–148 °C.

4.13. Reaction of $[Cp^*(CO)_2Fe(HMTA)]BF_4$ with $[Cp(CO)_2Fe(OEt_2)]BF_4$ in dichloromethane at room temperature

Into a stirred solution of $[Cp^*(CO)_2Fe(HMTA)]BF_4$ (0.147 g, 0.31 mmol) in CH_2Cl_2 (10 ml), a solution of (**1**) (0.117 g, 0.35 mmol) in CH_2Cl_2 (10 ml) was added within 3 min using a cannula. The mixture was stirred overnight at room temperature after which an orange solid stuck to the walls of the Schlenk tube. The mixture

was filtered into a clean and dry Schlenk tube and the residue washed with CH_2Cl_2 (4 × 5 ml) to give 0.087 g of orange solid, which by NMR and IR was found to be a mixture of $[Cp(CO)_2Fe(HMTA)]BF_4$ and $[\{Cp(CO)_2Fe\}_2\mu\text{-}(HMTA)](BF_4)_2$. Into the filtrate, diethyl ether 30 ml was added and the mixture was allowed to stand overnight. After this period no precipitate formed and therefore the solvent was removed under reduced pressure to give a deep red oil which was found to be a mixture of decomposed Cp^* and Cp compounds as was suggested by the ^1H NMR spectrum which show numerous peaks in the Cp^* and Cp regions.

4.14. Reaction of $[Cp^*(CO)_2Fe(HMTA)]BF_4$ with $[Cp(CO)_2Fe(OEt_2)]BF_4$ in dichloromethane at 0 °C

To a pre-cooled solution of $[Cp^*(CO)_2Fe(HMTA)]BF_4$ (0.138 g, 0.29 mmol) in CH_2Cl_2 (10 ml) at −78 °C, a solution of $[Cp(CO)_2Fe(OEt_2)]BF_4$ (0.102 g, 0.30 mmol) in CH_2Cl_2 (10 ml) was added and the mixture allowed to warm to 0 °C. It was then stirred at this temperature for 1 h after which an orange solid stuck on the walls of Schlenk tube. The mixture was filtered and the residue washed with CH_2Cl_2 portions until the washings were almost colourless. The residue was then dried under reduced pressure to give 0.034 g of an air sensitive orange spongy solid of the dinuclear complex $[\{Cp(CO)_2Fe\}(\mu\text{-}HMTA)\{Fe(CO)_2Cp^*\}](BF_4)_2$. ^1H NMR (400 MHz, CD_3CN): 5.46 (s, 5H, C_5H_5), 4.63–4.4.23 (m, 12H, HMTA), 1.81 (s,15H, $C_5(CH_3)_5$). $^{13}C\{^1H\}$ NMR (400 MHz, CD_3CN): δ 86.38 (C_5H_5), 86.73 (C2), 83.43 (C4, C9), 80.17 (C8, C10), 68.48 (C6), 8.38 ($C_5(\underline{C}H_3)_5$), 99.00 ($\underline{C}_5(CH_3)_5$).209.78, 208.62 (CO).

4.15. Single-crystal X-ray data

Crystals of $[Cp^*(CO)_2Fe(1\text{-}meIm)]BF_4$, $[Cp(CO)_2Fe(1\text{-}meIm)]BF_4$ and $[\{Cp^*(CO)_2Fe\}_2(\mu\text{-}HMTA)](BF_4)_2$ suitable for X-ray diffraction studies were obtained by different methods of crystal growth as described below:

4.15.1. Crystallization of $[Cp^*(CO)_2Fe(1\text{-}meIm)]BF_4$

A filtered and nitrogen-saturated solution of $[Cp^*(CO)_2Fe(1\text{-}meIm)]BF_4$ in dry CH_2Cl_2 was layered with dry and degassed diethyl ether. The mixture was kept undisturbed in the dark at room temperature. Yellow crystals were obtained over 3 days of liquid diffusion under strict anaerobic conditions.

4.15.2. Crystallization of $[Cp(CO)_2Fe(1\text{-}meIm)]BF_4$

Vapours of dry diethyl ether were allowed to diffuse into a filtered solution of $[Cp(CO)_2Fe(1\text{-}meIm)]BF_4$ in dry CH_2Cl_2 and the mixture allowed to stand undisturbed and under strict anaerobic conditions for a period of one month in the dark at 5 °C. This gave yellow crystals suitable for X-ray diffraction.

4.15.3. Crystallization of $[\{Cp^*(CO)_2Fe\}_2(\mu\text{-}HMTA)](BF_4)_2$

Crystals of $[\{Cp^*(CO)_2Fe\}_2\{\mu\text{-}HMTA)](BF_4)_2$ suitable for the X-ray diffraction study were grown by slow evaporation of acetonitrile solution at 279 K over a period of 4 weeks.

Intensity data were collected on a Bruker *APEX II CCD* area detector diffractometer with graphite monochromated Mo Ka radiation (50 kV, 30 mA) using the *APEX II* [70] data collection software. The collection method involved x-scans of width 0.5° and 512 × 512 bit data frames. Data reduction was carried out using the program SAINT+ [71] and face indexed absorption corrections were made using XPREP [71]. The crystal structure was solved by direct methods using SHELXTL [72]. Non-hydrogen atoms were first refined isotropically followed by anisotropic refinement by full matrix least-squares calculations based on F^2 using SHELXTL. Hydrogen atoms were first located in the difference map then positioned geometrically and allowed to ride on their respective parent atoms. Diagrams and publication material were generated using SHELXTL, PLATON [73] and ORTEP-3 [74]. Table 2 summarizes crystal data and structure refinement information while selected bond length and angles are given in Tables 1, 3 and 4.

Acknowledgments

We sincerely thank the NRF, THRIP and UKZN (URF) for financial support. The assistance of Dr. Manuel Fernandes (University of the Witwatersrand) with the X-ray data collection and solution is highly appreciated.

Appendix A. Supplementary material

CCDC 844986, 844987 and 844988 contains the supplementary crystallographic data for compounds **3a**, **7**, and **8**, respectively. These data can be obtained free of charge from The Cambridge Crystallographic Data Centre via www.ccdc.cam.ac.uk/data_request/cif. Supplementary data associated with this article can be found, in the online version, at http://dx.doi.org/10.1016/j.ica.2012.04.003.

References

[1] R.P. Nair, T.H. Kim, B.J. Frost, Organometallics 28 (2009) 4681.
[2] A. Rossin, L. Gonsalvi, A.D. Phillips, O. Maresca, A. Lledós, M. Peruzzini, Organometallics 26 (2007) 3289.
[3] E.M. Peña-Méndez, B. González, P. Lorenzo, A. Romerosa, J. Havel, Rapid Commun. Mass Spectrom. 23 (2009) 3831.
[4] C.A. Mebi, B.J. Frost, Organometallics 24 (2005) 2339.
[5] W.H. Ang, A. Casini, G. Sava, P.J. Dyson, J. Organomet. Chem. 696 (2011) 989.
[6] M. Xue, G. Zhu, H. Ding, L. Wu, X. Zhao, Z. Jin, S. Qiu, Cryst. Growth Des. 9 (2009) 1481.
[7] A.D. Phillips, L. Gonsalvi, A. Romerosa, F. Vizza, M. Peruzzini, Coord. Chem. Rev. 248 (2004) 955.
[8] J. Bravo, S. Bolan~o, L. Gonsalvi, M. Peruzzini, Coord. Chem. Rev. 254 (2010) 555.
[9] G. Kovács, L. Nádasdi, G. Laurenczy, F. Joó, Green Chem. 5 (2003) 213.
[10] D.J. Darensbourg, F. Joó, M. Kannisto, A. Kathó, J.H. Reibenspies, D.J. Daigle, Inorg. Chem. 33 (1994) 200.
[11] D.A. Krogstad, A.J. Deboer, W.J. Rudolf, J.A. Halfen, Inorg. Chem. Commun. 8 (2005) 1141.
[12] L. Gonsalvi, M. Peruzzini, Aqueous Phase Reactions Catalysed by Transition Metal Complexes of 7-Phospha-1,3,5-triazaadamantane (PTA) and Derivatives. Phosphorus Compounds, vol. 37, Springer, Netherlands, p. 183.
[13] M. Erlandsson, V.R. Landaeta, L. Gonsalvi, M. Peruzzini, A.D. Phillips, P.J. Dyson, G. Laurenczy, Eur. J. Inorg. Chem. (2008) 620.
[14] C. Lidrissi, A. Romerosa, Mustapha Saoud, M. Serrano-Ruiz, A. Luca Gonsalvi, M. Peruzzini, Angew. Chem., Int. Ed. 44 (2005) 2568.
[15] M.S. Ruiz, A. Romerosa, B. Sierra-Martin, A. Fernandez-Barbero, Angew. Chem., Int. Ed. 47 (2008) 8665.
[16] H.V. Huynh, Y.X. Chew, Inorg. Chim. Acta 363 (2010) 1979.
[17] J.G.J. Strom, H.W. Jun, J. Pharm. Sci. 75 (1986) 416.
[18] S.D. Greenwood, Infection 9 (1981) 223.
[19] A. Duthod, C.R. Seances, Soc. Bio. Fil. 111 (1932) 721.
[20] J. Bango, J. Joseph, L. Browman, PCT, WO 2010/120489A120482, 2010.
[21] V.G. Wong, L.L. Wood, P. Nixon, US Patent Pub No. 20080038316A20080038311, 2008.
[22] J.A. Giordano, US Patent Pub. No. 2009/0111780 A0111781, 2009.
[23] S. Masunaga, K. Tano, J. Nakamura, M. Watanabe, G. Kashino, A. Takahashi, H. Tanaka, M. Suzuki, K. Ohnishi, Y. Kinashi, Y. Liu, T. Ohnishi, K. Ono, J. Radiat. Res. 51 (2010) 27.
[24] B.B. García, D. Liu, S. Sepehri, S. Candelaria, D.M. Beckham, L.W. Savage, G. Cao, J. Non-Cryst. Solids 356 (2010) 1620 (and refs. therein).
[25] B. Baghernejad, Eur. J. Chem. 1 (2010) 54.
[26] Y. Hon, C. Kao, Tetrahedron Lett. 50 (2009) 748 (and refs. therein).
[27] F. Zhang, X. Wang, C. Cai, J. Liu, Tetrahedron 65 (2009) 83.
[28] W. Shieh, S. Dell, A. Bach, O. Repíc, T.J. Blacklock, J. Org. Chem. 68 (2003) 1954.
[29] E. Gordon, J. Cohen, R. Engel, G.W. Abbott, Mol. Pharmacol. 69 (2006) 718.
[30] R.M. Matos, J.G. Verkade, J. Braz. Chem. Soc. 14 (2003) 71.
[31] L.E. Kapinos, B. Song, H. Sigel, Chem. Eur. J. 5 (1999) 1794.
[32] M.S. Szulmanowicz, W. Zawartka, A. Gniewek, A.M. Trzeciak, Inorg. Chim. Acta 363 (2010) 4346.
[33] H. Nakamura, M. Fujii, Y. Sunatsuki, M. Kojima, N. Matsumoto, Eur. J. Inorg. Chem. (2008) 1258.
[34] R. Sívek, F. Burěs, O. Pytela, J. Kulhānek, Molecules 13 (2008) 2326.

[35] A.N. Nasmeyanov, Y.A. Belousov, V.N. Babin, G.G. Aleksandrov, Y.T. Struchkov, N.S. Kochetkova, Inorg. Chim. Acta 23 (1977) 155.
[36] H. Tchouka, A. Meetsma, W.R. Browne, Inorg. Chem. 49 (2010) 10557.
[37] S. Wen-Hua, X. Tang, T. Gao, B. Wu, W. Zhang, H. Ma, Organometallics 23 (2004) 5037.
[38] S. Wen-Hua, S. Jie, S. Zhang, W. Zhang, Y. Song, H. Ma, J. Chen, K. Wedeking, R. Fröhlich, Organometallics 25 (2006) 666.
[39] S. Wen-Hua, P. Hao, S. Zhang, Q. Shi, W. Zuo, X. Tang, X. Lu, Organometallics 26 (2007) 2720.
[40] S. Zhang, S. Wen-Hua, T. Xiao, X. Hao, Organometallics 29 (2010) 1168.
[41] E.O. Changamu, H.B. Friedrich, M. Rademeyer, J. Organomet. Chem. 693 (2008) 164.
[42] E.O. Changamu, H.B. Friedrich, M. Rademeyer, J. Organomet. Chem. 692 (2007) 2456.
[43] E.O. Changamu, H.B. Friedrich, J. Organomet. Chem. 692 (2007) 1138.
[44] C.M. M'thiruaine, H.B. Friedrich, E.O. Changamu, M.D. Bala, Inorg. Chim. Acta 366 (2011) 105.
[45] E.O. Changamu, H.B. Friedrich, M. Rademeyer, Acta Crystallogr., Sect. E 62 (2006) m442.
[46] E.O. Changamu, H.B. Friedrich, M.O. Onani, M. Rademeyer, J. Organomet. Chem. 691 (2006) 4615.
[47] E.O. Changamu, H.B. Friedrich, J. Organomet. Chem. 693 (2008) 3351.
[48] C.M. M'thiruaine, H.B. Friedrich, E.O. Changamu, B. Omondi, Acta Crystallogr., Sect. E 67 (2011) m485.
[49] M. Akita, S. Kakuta, S. Sugimoto, M. Terada, M. Tanaka, Y. Moro-oka, Organometallics 20 (2001) 2736.
[50] C.M. M'thiruaine, H.B. Friedrich, E.O. Changamu, M.D. Bala, Inorg. Chim. Acta 382 (2012) 27.
[51] A. Banerjee, P. Maiti, T. Chattopadhyay, K.S. Banu, M. Ghosh, E. Sureh, E. Zangrando, D. Das, Polyhedron 29 (2010) 951.
[52] A. Romerosa, T. Campos-Malpartida, C. Lidrissi, M. Saoud, M. Serrano-Ruiz, M. Peruzzini, J.A. Gárrido-cardenas, F. Garciá-Maroto, Inorg. Chem. 45 (2006) 1289.
[53] M.Y. Darensbourg, D. Daigle, Inorg. Chem. 14 (1975) 1217.
[54] D.C. Calabro, J.L. Hubbard, C.H. Blevins, A.C. Campbell, D.L. Lichtenberger, J. Am. Chem. Soc. 103 (1981) 6839.
[55] C.M. M'thiruaine, H.B. Friedrich, E.O. Changamu, M.D. Bala, Acta Crystallogr., Sect. E 67 (2011) m924.
[56] L.N. Becka, D.W.J. Cruickshank, Proc. R. Soc. A 273 (1963) 435.
[57] F. Hanic, V. Šubrtová, Acta Crystallogr., Sect. B 25 (1969) 405.
[58] B.J. Frost, C.A. Mebi, P.W. Gingrich, Eur. J. Inorg. Chem. (2006) 1182.
[59] B.J. Frost, C.M. Bautista, R. Huang, J. Shearer, Inorg. Chem. 45 (2006) 3481.
[60] S. Otto, A. Roodt, Inorg. Chem. Commun. 4 (2001) 49.
[61] T. Ljungdahl, K. Pettersson, B. Albinson, J. Mantensson, J. Org. Chem. 71 (2006) 1677.
[62] R.J. Sundberg, B. Martin, Chem. Rev. 74 (1974) 471.
[63] M. Powell, R.D. Bailey, C.T. Eagle, G.L. Schimek, T.W. Hanks, W.T. Pennington, Acta Crystallogr., Sect. C 53 (1997) 1611.
[64] J.D. Oliver, D.F. Mullica, B.B. Hutchinson, W.O. Milligan, Inorg. Chem. 19 (1980) 165.
[65] H. Schumann, M. Speis, W.P. Bosman, J.M.M. Smits, P.T. Beurskens, J. Organomet. Chem. 403 (1991) 165.
[66] J. Li, S.M. Nair, B.C. Noll, C.E. Schulz, W.R. Scheidt, Inorg. Chem. 47 (2008) 3841.
[67] Y. Zhang, W.A. Hallows, W.J. Ryan, J.G. Jones, G.B. Carpenter, D.A. Sweigart, Inorg. Chem. 33 (1994) 3306.
[68] Z.N. Zahran, N. Xu, D.R. Powell, G.B. Richter-Addo, Acta Crystallogr., Sect. E 65 (2009) m75.
[69] M. Akita, M. Tarada, M. Tanaka, Y. Morooka, J. Organomet. Chem. 510 (1996) 255.
[70] BRUKER, APEX2, Version 2009.1-0. Bruker AXS Inc., Madison, Wisconsin, USA, 2005.
[71] BRUKER, SAINT+, Version 7.60A (includes XPREP and SADABS) Bruker AXS Inc., Madison, Wisconsin, USA, 2005.
[72] BRUKER, SHELXTL, Version 5.1. (includes XS, XL, XP, XSHELL) Bruker AXS Inc., Madison, Wisconsin, USA, 1999.
[73] A.L. Spek, J. Appl. Crystallogr. 36 (2003) 7.
[74] L.J. Farrugia, J. Appl. Crystallogr. 30 (1997) 565.